






Article

Crystal Structure, Topological and Hirshfeld Surface Analysis of a Zn(II) Zwitterionic Schiff Base Complex Exhibiting Nonlinear Optical (NLO) Properties Using Z-Scan Technique

Saima Kamaal¹, Mohd Mehkoom² , Mohd Muslim¹ , Syed Mohammad Afzal², Abdullah Alarifi³, Mohd Afzal³ , Ahmad Alowais³, Mohd Muddassir^{3,*} , Awad Naseer Albalwi³ and Musheer Ahmad^{1,*} 

¹ Department of Applied Chemistry, ZHCET, Faculty of Engineering and Technology, Aligarh Muslim University, Aligarh UP-202002, India; saimakamaal786@gmail.com (S.K.); mohammadmuslim1996@gmail.com (M.M.)

² Department of Physics, Aligarh Muslim University, Aligarh UP-202002, India; mehkoomb@outlook.com (M.M.); drsmafzal62@gmail.com (S.M.A.)

³ Department of Chemistry, College of Science, King Saud University, Riyadh 11451, Saudi Arabia; arifi@ksu.edu.sa (A.A.); maslam1@ksu.edu.sa (M.A.); alowais@ksu.edu.sa (A.A.); awad_albalwi@hotmail.com (A.N.A.)

* Correspondence: mmohammadarshad@ksu.edu.sa (M.M.); amusheer4@gmail.com (M.A.)



Citation: Kamaal, S.; Mehkoom, M.; Muslim, M.; Afzal, S.M.; Alarifi, A.; Afzal, M.; Alowais, A.; Muddassir, M.; Albalwi, A.N.; Ahmad, M. Crystal Structure, Topological and Hirshfeld Surface Analysis of a Zn(II) Zwitterionic Schiff Base Complex Exhibiting Nonlinear Optical (NLO) Properties Using Z-Scan Technique. *Crystals* **2021**, *11*, 508. <https://doi.org/10.3390/cryst11050508>

Academic Editors: Assem Barakat and Alexander S. Novikov

Received: 5 April 2021

Accepted: 1 May 2021

Published: 4 May 2021

Publisher's Note: MDPI stays neutral with regard to jurisdictional claims in published maps and institutional affiliations.



Copyright: © 2021 by the authors. Licensee MDPI, Basel, Switzerland. This article is an open access article distributed under the terms and conditions of the Creative Commons Attribution (CC BY) license (<https://creativecommons.org/licenses/by/4.0/>).

Abstract: A mononuclear Zn(II) complex of (Zn(H₂L)(CH₃OH)Cl₂) (**1**) has been synthesized by using a nonlinear optically active Zwitterionic Schiff base which is 4-((2-hydroxy-3-methoxybenzylidene)amino) benzoic acid (H₂L). Complex **1** has been structurally analyzed by FTIR and UV spectroscopy, TGA, Powder-XRD and single crystal X-ray diffraction. X-Ray crystallographic studies revealed Zn(II) complex crystallizes in a *P21/c* space group and exists in a distorted trigonal bipyramidal geometry ($\tau = 0.68$). The topological analysis of complex **1** showed that the underlying net is characterized by an unknown topological type and point symbol {3⁴².4⁶⁸.5¹⁰}, and multilevel analysis of complex packing as dimer gives a 18-c uninodal net with unknown topological type and point symbol {3⁴⁸.4⁹⁹.5⁶}. The calculation results of a Hirshfeld surface analysis have been investigated to explore the H-bonding within the crystal. Third-order non-linear properties were also studied, which revealed that the lower input power (5.0 mW) for the material shows full transparency; however, it becomes opaque for higher input power. Such limiting behavior of complex **1** suggests its potential for instrumental protective devices against high laser illuminations.

Keywords: Zn(II) complex; zwitterion; single crystal XRD; Hirshfeld surface analysis; third-order NLO

1. Introduction

In the recent development of third-order nonlinear optical (NLO) based inorganic materials have been widely used in applications such as in photonic devices like telecommunications, optical computing, optical storage, and optical information processing optoelectronics, medical etc. [1–3]. Nonlinear optical effects arise upon the exposure of high intensity of lesser light to the optical material, and thus act as an influential part in the delocalization of π -electrons by light exposure [4,5]. There are double key aspects which regulate the NLO response of molecules such as (a) electron donor and acceptor π -electron conjugated arrangement as a connection providing the electronic link between them and, (b) the connection structure unit should be packed in a non-centrosymmetric way [6]. Literature reports revealed that 3d-transition metal complexes have increased attention in the third-order nonlinear optical response over the non-coordination molecules due to their (a) wide range of molecular structure assembly, (b) diversity of coordination environment exhibited by the metal center [7–9]. Moreover, the scheme of building new third-order non-linear optical active materials required for applied applications is still a decidedly challenging task.

Among a variety of π -conjugated organic ligands, Schiff bases bearing nitrogen and oxygen donor atoms have appeared as promising molecules for nonlinear optical materials on explanation of the π -electron bridge from carbon–nitrogen double bonds (C=N), which plays a critical role in enhancing the molecular NLO response [8,10–12]. It is evident that the third-order NLO susceptibility increases with the length of conjugation within a molecule, because they can afford convenient electronic transfer passage and the delocalization of π -electrons throughout the molecular system [11,13,14]. Additionally, the planar aromatic ring connected through the π -electron bridge (C=N) acts as an ideal candidate for large and fast optical nonlinearities materials. This is due to the fact that these compounds hold the extended mobile π -electron clouds over molecular distances and are easily polarized [15]. In this context, Schiff base metal complexes have shown to be of immense interest for the building of NLO materials. Therefore, several Schiff base ligands have been used to study their electronic structure and nonlinear optical properties [16,17]. One of the NLO behavior is the third harmonic generation (THG), where light of angular frequency (ω) is converted into light at three times higher angular frequency (3ω) upon absorption by the nonlinear optical material [18]. In the recent past, investigations on the NLO properties of materials for optical limiting (OL) behavior have been motivated by the need to guard sensitive photonic devices and human eyes from exposure to high intensity laser light [19,20]. By tuning the factors affecting the nonlinear behavior, specifically the ease of processability, the uniqueness of metal ions, and changing the symmetry of the molecule, it is possible to modulate the nonlinear response along with optical limiting performance of a material [21,22].

To date, Zn(II) Schiff-base complexes have been examined for their interesting photophysical and third-order nonlinear optical properties [23,24]. The choice of zinc(II) as the metal center is an important prerequisite for such applications, as its transparency avoids absorption of the second harmonic in a large spectral range due to the absence of d–d transitions, and it exhibits the largest hyperpolarizability [25]. Nevertheless, the zinc(II) metal ion, due to its Lewis acidity, flexible coordination number (ranges from four to six) and lack of redox behavior, has long been recognized as an important co-factor in several biological systems [26]. Furthering the aim of understanding the Zwitterionic Schiff base towards NLO response [27], herein, we report the synthesis, structural characterization and interesting structural topological behavior of the Zn(II) coordination complex through explored its NLO properties. We have also measured the nonlinear refractive index (n_2), nonlinear absorption coefficient (β) and third-order optical susceptibility, $\chi^{(3)}$, by the Z-scan method. Moreover, the supramolecular network is also probed by the Hirshfeld surface analysis.

2. Material and Methods

2.1. Reagents and Materials

All the chemicals and solvents were commercially purchased and used without further purification. Reagent grade 2-Hydroxy-3-methoxybenzaldehyde and 4-aminobenzoic acid and zinc chloride tetrahydrate was procured from Sigma-Aldrich, and Methanol was procured from S.D. Fine Chemicals, India.

2.2. Methods and Instrumentation

Infrared spectrum was collected (KBr disk, 400–4000 cm^{-1}) by using a Perkin-Elmer Model 1320 spectrometer. Thermogravimetric analyses (TGA) were acquired on a Mettler Toledo Star System (heating rate of 10 $^{\circ}\text{C}/\text{min}$). Elemental analysis was done using a CE-440 elemental analyzer (Exeter Analytical Inc.). Powder X-ray diffraction measurements ($\text{CuK}\alpha$ radiation, scan rate 3 $^{\circ}/\text{min}$, room temperature) were performed on a Bruker D8 Advance Series 2 powder X-ray diffractometer.

2.3. Synthesis

2.3.1. Synthesis of (H₂L)

4-((2-hydroxy-3-methoxybenzyl)amino)benzoic acid ligand was synthesized following the previously described method [28]. 2-Hydroxy-3-methoxybenzaldehyde (7.2 mmol) was added to the hot solution of 4-Aminobenzoic acid (7.2 mmol) in 15 mL methanol. The reaction mixture was heated for about another 30 min until the completion of the reaction. Then, it was filtered and repeatedly washed with hot methanol and dried under vacuum. Yield (~78%). It was crystallized by slow evaporation in methanol. M.P. 254–255 °C, FT-IR (KBr cm⁻¹): 3422(s) 2917(s), 2837(m), 2536(m), 1691(s), 1593(m), 1462(s), 1421(s), 1364(s), 1288(s), 1252(s), 1166(m), 1169(s), 1099(m), 1016(s), 967(s), 853(s), 745(s), 731(s), 691(m). UV-vis absorption: (λ_{\max} , nm): 315 nm.

2.3.2. Synthesis of [Zn(H₂L) (CH₃OH) Cl₂] (1)

Solution of ZnCl₂·4H₂O (0.136 g, 0.5 mmol) in 15 mL methanol was slowly added to a hot stirring solution of H₂L (0.271 g, 1 mmol) in 15 mL methanol. The mixture was stirred at room temperature for 6 h. The resulting mixture was subsequently filtered and slowly evaporated at room temperature. Orange colored block shaped crystal suitable for single crystal diffraction was obtained after 1 week. Yield: 74%; m.p. > 340 °C. Anal. (%) Calc. for C₁₆H₁₇Cl₂NO₅ Zn: C, 43.71; H, 3.89; N, 3.18. Found: C, 43.85; H, 3.73; N, 3.19. FT-IR (KBr pellet: cm⁻¹): 3438 (s, O-H), 2918 (m, C-H), 1678 (m, C=N), 1246 (s, C-O), 1260, 1245, 1140 (m, Ph-OH), 498, 545 (w, Zn-O). UV-Vis [C₂H₅OH; λ_{\max} /nm]: 344 nm (Supplementary Material, Figures S1 and S2).

The details of X-ray crystal refinement, topological and Hirshfeld surface analysis have been moved to supporting information (See the Supplementary Materials).

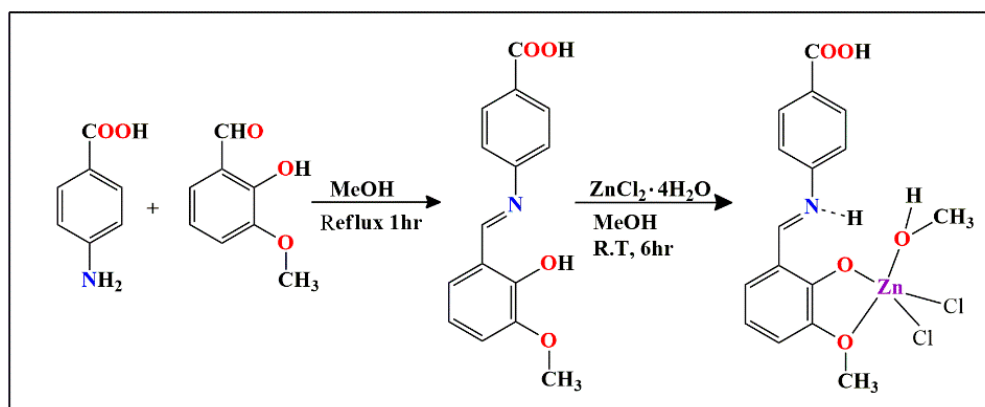
2.4. Z-Scan Method

To find out the third-order NLO characteristics of complex **1** the Z-scan technique [29] was employed with a Gaussian beam CW diode laser (Thorlabs) operating at 520 nm. Herein the laser beam was focused at a sample using a convex lens of 50 mm focal length, and the sample was translated along the beam propagation axis (say Z-axis) at a long travel stage (LTS150/M, Thorlabs) of 150 mm length. The sample was prepared in ethanol at a solution concentration of 5.0 Mm. When the sample poured in the cuvette of 1 mm thickness is translated, it behaves like a thin lens fulfilling the conditions of a thin lens [30]. Further, an aperture was placed before a photomultiplier tube (PMM01-1, Thorlabs) kept at far-field. The signal transmitted through the sample was detected using PMT via aperture for close and open scans. The signal was digitalized using an A/D converter (Leybold, Sensor Cassy-2) and stored in a computer in the form of transmittance. The detailed information on the Z-scan setup can be seen in our reported articles [27,31].

3. Results and Discussion

3.1. Synthesis and Characterization

The present examination aims to ascertain the role of Zwitterionic Schiff base, namely 4-((2-hydroxy-3-methoxybenzylidene) amino) benzoic acid (H₂L) in the mononuclear Zn(II) complex **1** on non-optical behavior using the Z-scan method, in order to determine both the nonlinear refractive index (n_2) and the nonlinear absorption coefficient (β). Of the various methods available, Z-scan technique is a simple and reliable tool for defining nonlinear properties of materials for optical limiting (OL). The proposed geometry of complex **1** was established by microanalytical, TGA, PXRD, FTIR, and electronic spectral studies. The single-crystal X-ray diffraction method reveals the distorted trigonal bipyramidal geometry around Zn(II) metal center. The reaction of H₂L with zinc chloride tetrahydrate in 1:1 molar ratio in methanol under reflux condition is depicted in Scheme 1). The complex is found to be air-stable and soluble in methanol, acetonitrile, DMSO and DMF.



Scheme 1. Synthetic scheme of 4-((2-hydroxy-3-methoxybenzyl)amino)benzoic acid (H_2L) and complex **1**.

The IR spectra for complex **1** is taken in from 4000 to 400 cm^{-1} . It exhibited a broad band in the region of 3438 cm^{-1} , which corresponds to the $\nu(\text{O-H})$ stretching vibration. The Schiff base molecule has a tendency to form zwitterionic forms via the transfer of a H-atom from OH group, forming $\text{N-H} \dots \text{O}^+$ intramolecular hydrogen bonding and its absorption band found from 3432 to 3449 cm^{-1} and presence of absorption peak at 1604 cm^{-1} for $\nu(\text{C=O})$. Further, there is no significant shift in the azomethine group $\nu(\text{C=N})$ 1678 cm^{-1} as compared the free ligand, which shows the azomethine group does not take part in coordination of the Zn-complex. A band appeared at 499 cm^{-1} , attributed to the M-O stretching vibration which attributes to the coordination of Zn-O .

UV-vis spectra of complex **1** were recorded in ethanol medium. Where the free ligand exhibited a peak at 315 nm , after the coordination of Zn-metal it is shifted to 344 nm , which may be attributed to $n \rightarrow \pi^*$.

3.2. Structure Description

Single-crystal X-ray structure determination revealed that complex **1** crystallizes in the monoclinic system in $P21/c$ space group with the four unit per cell (Table 1). Its asymmetric unit consists of a mononuclear zinc(II) center coordinated to a Schiff base ligand, chloride ion and methanol. ORTEP view of asymmetric unit is depicted in Figure 1. Complex contains a penta-coordinated mononuclear zinc (II) ion, which has distorted trigonal bipyramidal geometry with Addison parameter $\tau = 0.68$ ($\tau = (\beta - \alpha)/60^\circ$ where: β and α are the two greatest valence angles of the coordination metal; $\tau = 1$ for perfect trigonal bipyramidal geometry) [32]. It is coordinated with the three O-atoms, two Schiff base ligands, with bond distance Zn1-O1 (1.99 \AA) and $\text{Zn1-O2}_{\text{methoxo}}$ (2.407 \AA) while one O-atom of methanol Zn1-O5 (2.11 \AA), and two chloride ions (bond distance of Zn-Cl1 , Zn-Cl2 is 2.25 \AA and 2.21 \AA , respectively). Bond distance of Zn-O and Zn-Cl are in the normal range for the Schiff base complex [33], while the $\text{Zn-O}_{\text{methoxo}}$ bond is larger than the average bond distance of $\text{Zn-O}_{\text{phenoxo}}$. The longer bond length of $\text{Zn-O}_{\text{methoxo}}$ as compared to $\text{Zn-O}_{\text{phenoxo}}$ shows that the $\text{Zn-O}_{\text{methoxo}}$ bond is weaker than the $\text{Zn-O}_{\text{phenoxo}}$ bond. This is due the steric hindrance caused by the methyl group to form closer bonds of the methoxy O-atom to the Zn(II) ion. In the crystal, the Schiff base molecule is in the zwitterionic form, which contributes to its structural stability forming $\text{N-H} \dots \text{O}$ intramolecular hydrogen bonding. The bond angles around Zn(II) ions are in the range of from 88 to 159° . Selected bond length and bond angles of complex **1** are listed in Table S1.

The detailed structural analysis shows that the crystal is not only stabilized by the coordination of the Zn(II) ion with ligands but also by the weak intermolecular H-bonding interaction of the Cl ion, and the carboxylate ion of the Schiff base. The mononuclear units are linked through classical H-bonding of the carboxylate ion $\text{O4-H4} \dots \text{O3}$ (1.64 \AA), and $\text{C4-H4a} \dots \pi$ interaction leads to generation of the 2D zig-zag layered structure shown in Figure 2. Further, the weak interaction formed by $\text{O-H} \dots \text{Cl}$ and $\text{C-H} \dots \text{Cl}$ ($\text{O5-H5} \dots$

Cl1 (2.30 Å), C13–H13 ... Cl1 (2.68 Å), C8–H8 ... Cl2 (2.78 Å), C10–H10 ... Cl1 (2.81 Å)) (Table 2) extends it to the 3D supramolecular structure.

Table 1. Crystal and structure refinement data for complex 1.

CCDC Number	2,075,253
Empirical formula	C ₁₆ H ₁₇ Cl ₂ NO ₅ Zn
Formula weight	439.61
Temperature/K	100(2)
Crystal system	Monoclinic
Space group	P21/c
a/Å	9.2547(11) Å
b/Å	31.069(4)
c/Å	6.3645(8)
α/°	90
β/°	103.797(4)
γ/°	90
Volume/Å ³	1777.2(4)
Z	4
ρ _{calc} /cm ³	1.6429
μ/mm ⁻¹	1.709
F(000)	898.8
Crystal size/mm ³	0.37 × 0.28 × 0.17
Radiation	MoKα (λ = 0.71073)
2θ range for data collection/°	4.54 to 50.08
Index ranges	−12 ≤ h ≤ 12, −41 ≤ k ≤ 41, −8 ≤ l ≤ 8
Reflections collected	27,216
Independent reflections	3150 [R _{int} = 0.1598, R _{sigma} = 0.1170]
Data/restraints/parameters	3150/0/235
GOF ^a on F ²	1.072
Final R indexes [I ≥ 2σ (I)]	R1 = 0.1093, wR2 = 0.2556
Final R ^b indexes [all data]	R1 = 0.1374, wR2 = 0.2745
Largest diff. peak/hole/e Å ⁻³	1.89/−3.18

^a GOF is defined as $\{\sum[w(F_0^2 - F_c^2)]/(n - p)\}^{1/2}$ where n is the number of data and p is the number of parameters.

^b $R_1 = \{\sum \|F_0 - |F_c|\| / \sum |F_0|\}$, $wR_2 = \{\sum w(F_0^2 - F_c^2)^2 / \sum w(F_0^2)\}^{1/2}$.

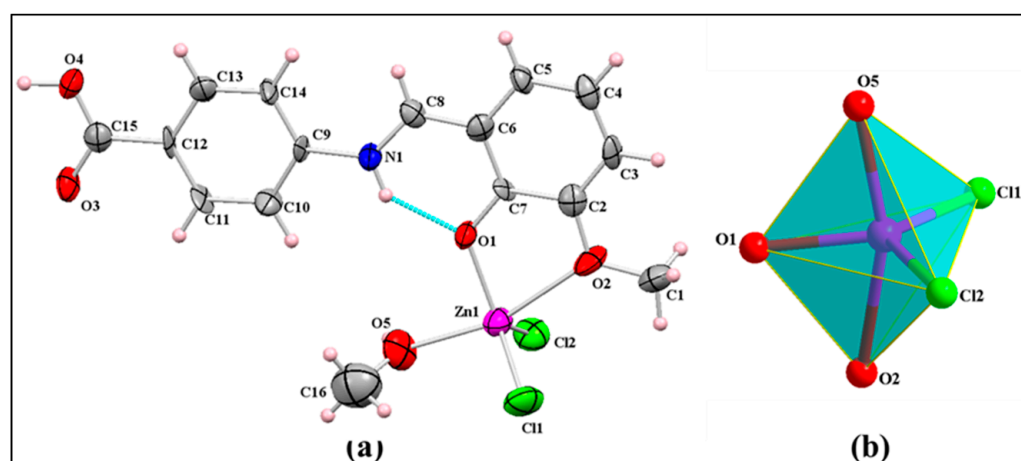


Figure 1. (a) ORTEP view of asymmetric unit of complex 1 at 70% probability level with labelled atoms. (b) A view of co-ordination environment around zinc(II) ion.

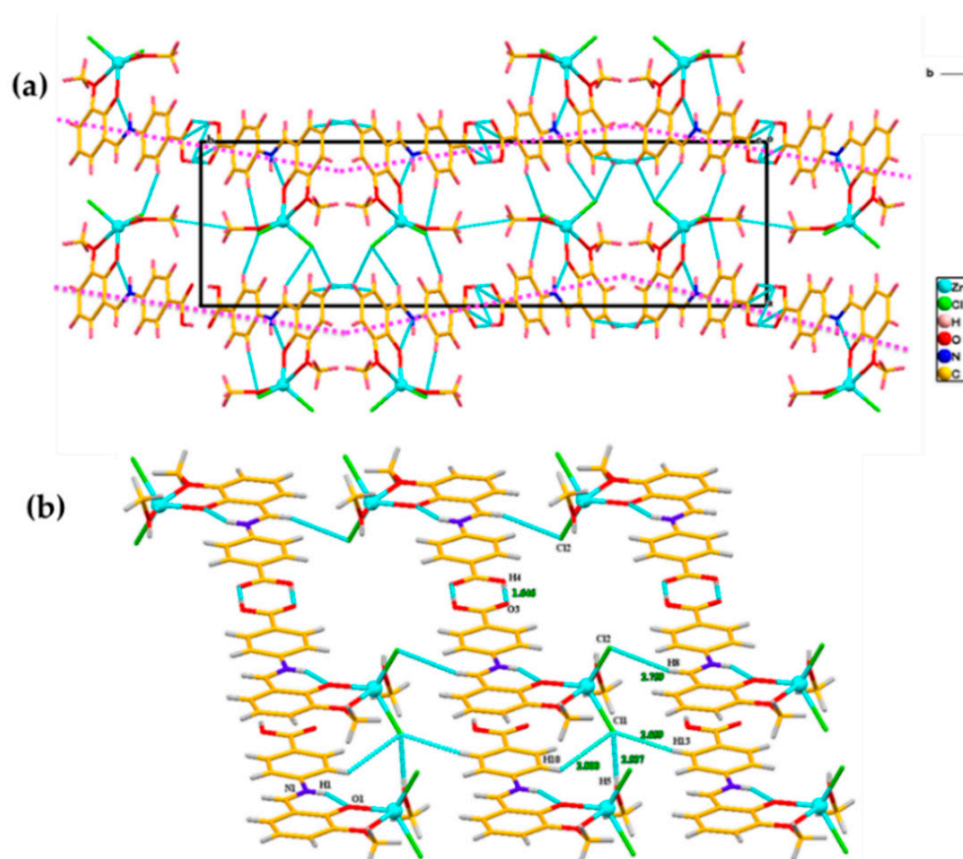


Figure 2. (a) A view of intermolecular and intramolecular interaction in the crystal packing along with the crystallographic axis *c* propagated H-bonding interactions. (b) A close view of H-bonding in complex 1, represented by dotted lines along with bond length within the crystal.

Table 2. Classical hydrogen bond geometry (Å) in crystal of complex 1.

D—H ... A	D—H	H ... A	D ... A	Label
Intra N(1)—H(1) ... O(1)	0.86	1.86	2.56 (3)	1
1 O(4)—H(4) ... O(3)	0.98	1.64	2.61 (3)	2-deep red spot
1 O(5)—H(5) ... Cl(1)	0.91	2.3	3.12 (4)	3-deep red spot
1 C(8)—H(8) ... Cl(2)	0.93	2.78	3.61 (5)	4-red spot
1 C(10)—H(10) ... Cl(1)	0.93	2.81	3.50 (5)	5-red spot
1 C(13)—H(13) ... Cl(1)	0.93	2.68	3.55 (5)	6-red spot
Intra 1 C(13)—H(13) ... O(4)	0.93	2.44	2.75 (4)	7

3.3. Topological Analysis

The topological analysis was done by the ToposPro program to study all atoms, especially the weakest links between them, which resemble the whole representation of a molecular framework. Other representation with a derived topology is partial, which can be labelled by subnet of an underlying net (UN), so-called standard simplification of the valence-bonded supramolecular network. Complex 1 displayed hydrogen bonds of the first type (1.846 Å), as an intramolecular bond. Hydrogen bonds of second type (1.646 Å) connected two molecules such as in dimers (1M2-1 topological type). Hydrogen bonds of third type, with chlorine, connected molecules in [001] direction, and form a chain. Subsequently, the resulting underlying net for this structure in standard representation H-bonded molecular MOFs is classified as 3-c net with (4,4) (0,2) topological type (Figure 3).

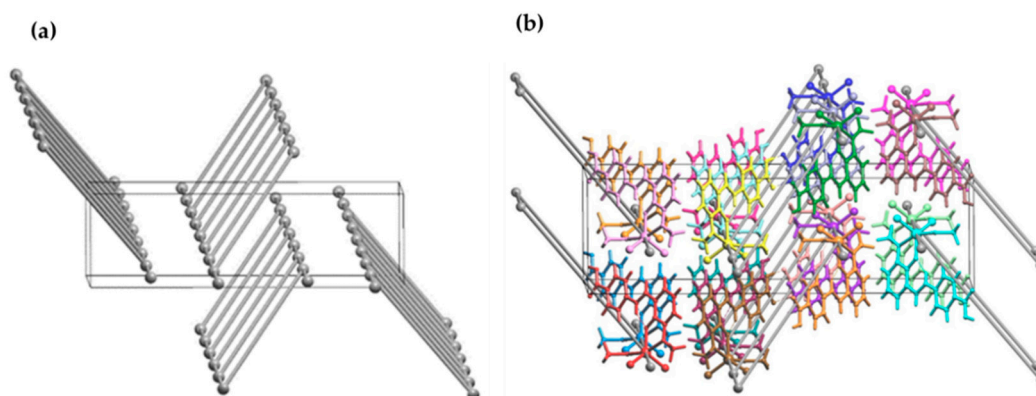


Figure 3. (a) Underlying net for the complex 1 crystal structure in standard representation of the H-bonded molecular MOFs and (b) Underlying net and fragment of crystal structure for complex 1.

The topological analysis of complex 1 involves the standard simplification procedure of the Coulomb or van der Waals bonded structure. Taking into account all intermolecular contacts during the simplification procedure, one can obtain a description of the molecular packing. The calculation results showed that the underlying net is characterized by an unknown topological type and point symbol $\{3^{42}.4^{68}.5^{10}\}$.

By means of the subroutine applied in ToposPro, different subnets were found from the underlying net that comprise the edges of a weight no less than a specified value. Having applied the multilevel analysis, we obtain the following order of the subnets that describe the packing of the structure on different levels of the solid angle (Supplementary Material; Table S5).

Packing of dimers (Figure 4 right) can be considered for complex 1. This is a 18-c uninodal net (Figure 4 left) with an unknown topological type and point symbol $\{3^{48}.4^{99}.5^6\}$. Generation of representation for this net is shown in Supplementary Materials, Table S6.

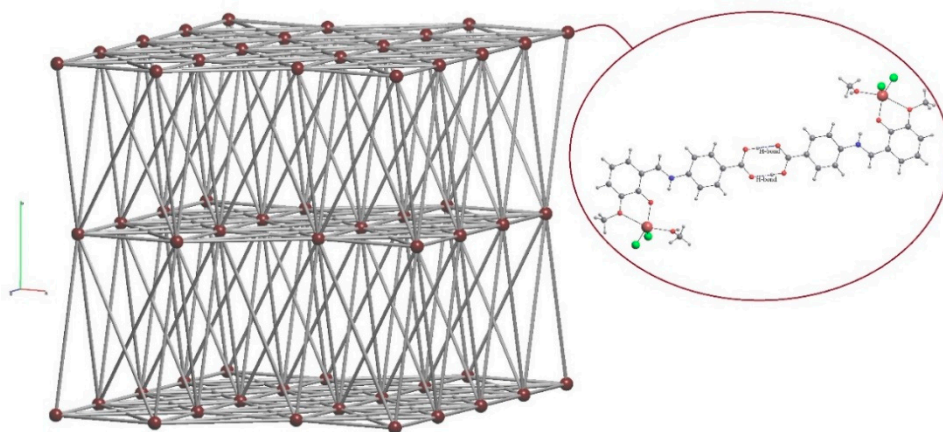


Figure 4. Underlying net for complex 1 for which the nodes represent its dimers.

3.4. Thermogravimetric Analyses (TGA) and Powder-XRD Patterns

TGA analysis was performed to investigate the thermal stability of complex 1 under N_2 atmosphere at $10\text{ }^\circ\text{C}/\text{min}$ in the temperature range $20\text{--}800\text{ }^\circ\text{C}$ (Figure 5). The thermogram curve of the Zn (II) complex displays three weight loss steps. The first weight loss is in the region from $63\text{ to }90\text{ }^\circ\text{C}$, and corresponds to the loss of coordination of methanol. Due to the departure of solvent molecules further decomposition begins. The second weight loss in the region from $200\text{ to }270\text{ }^\circ\text{C}$ shows loss of coordination of chloride ions. The third weight loss in the region from $271\text{ to }680\text{ }^\circ\text{C}$ corresponds to the gradual decomposition of the Schiff base ligand and residual formation of ZnO .

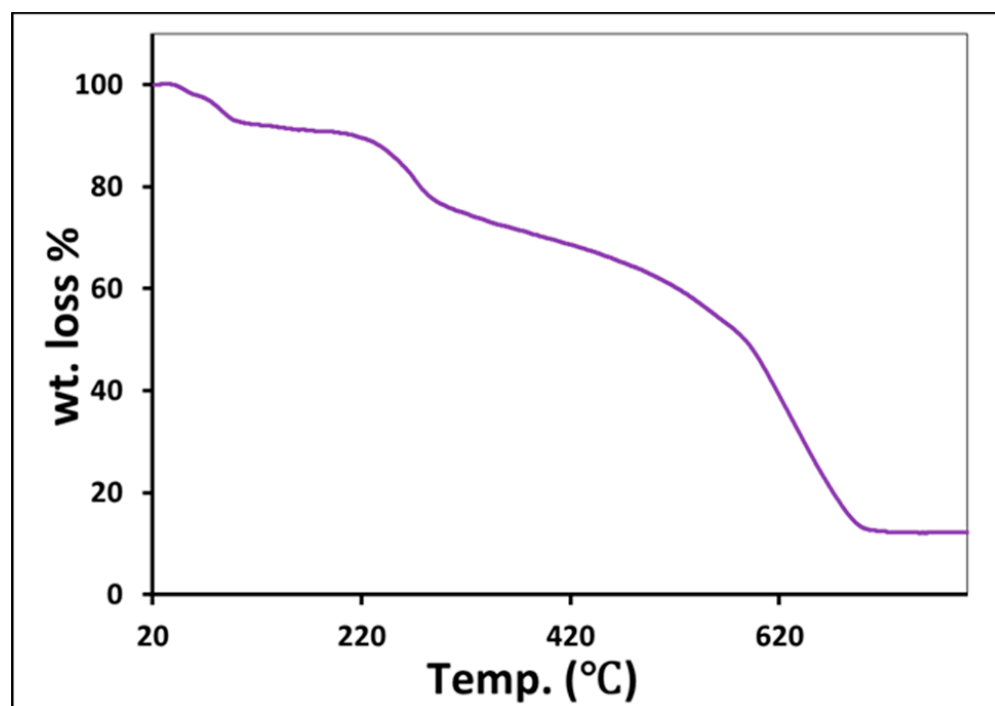


Figure 5. Thermogravimetric analysis (TGA) of complex 1.

Here, we have performed PXRD analysis to look over the crystalline nature of complex 1 in bulk phase in the range from 5.0 to 40.00 (2θ). The PXRD pattern of complex 1 matches with the stimulated pattern obtained from single crystal-XRD. This confirms the stability of the crystalline nature of the complex in bulk phase (Figure 6).

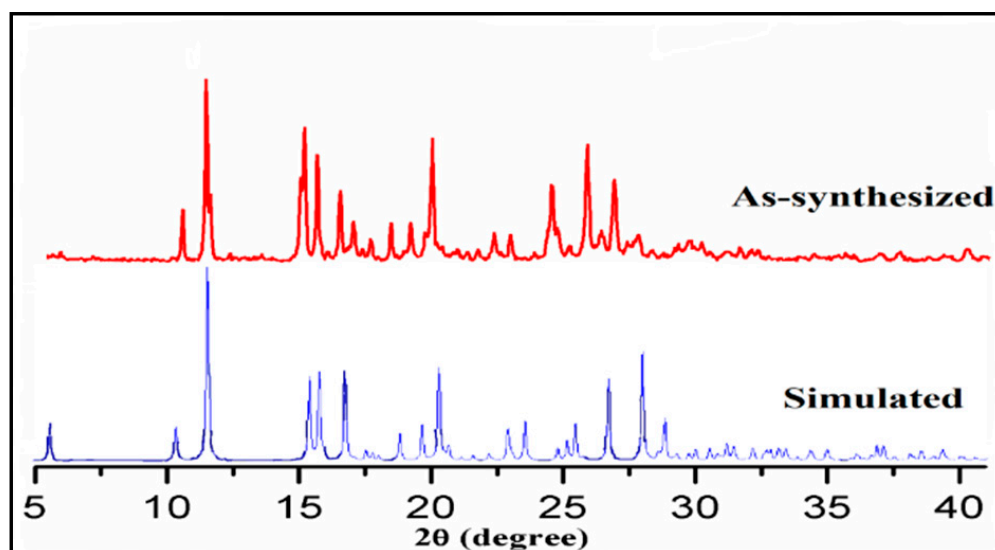


Figure 6. PXRD patterns of simulated (Blue) and synthesized (red) from complex 1.

3.5. Hirshfeld Surface Analysis

For complex 1, Hirshfeld surface analysis for complex 1 is mapped over d_{norm} (normalize contact distance) in the color range from 0.758 to 1.742 a.u (Figure 7), which indicates the different close contacts with neighboring species of the molecule. The d_{norm} image is made transparent for visualizing the molecular structure of complex 1, where d_{norm} shows the different region of different color scheme ,i.e., red, white and blue. Deep red spots are

indicating the strong close interaction with the neighboring species that are listed in Table 2. Spots 2 and 3 revealed classical O–H···O and O–H···Cl bonding, respectively, in the crystal of complex 1. Beside this, some light red spots, 5, 6 and 9 are corresponding to C–H···Cl and CH–CH interactions and other visible spots are corresponding to C–H··· π interaction with neighboring species. Hirshfeld surface analysis is also mapped over shape index and curvedness in complex 1.

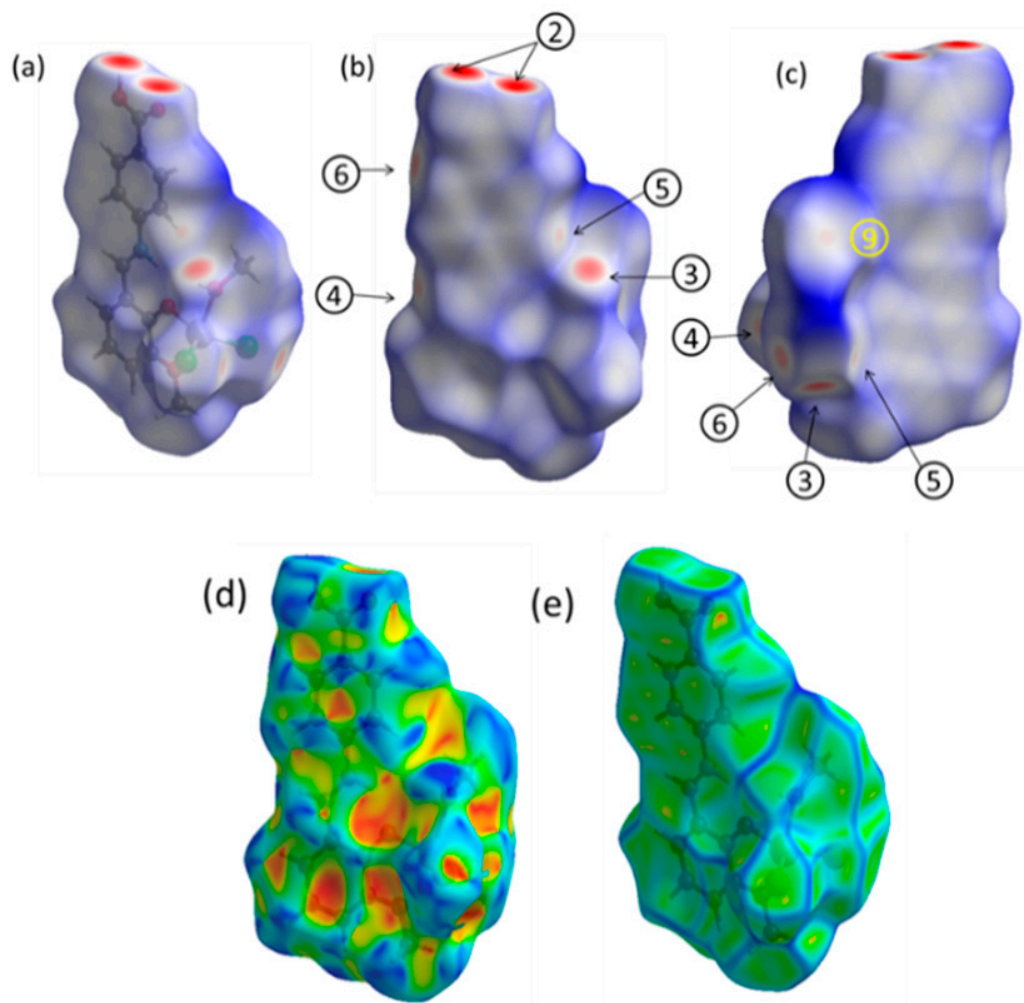


Figure 7. Representation of (a) Transparent for better visualization, (b) Front (c) back view of Hirshfeld surface mapped over d_{norm} in the color range from 0.758 to 1.742. (d) shape index (e) curvedness of complex 1. Labels are referring to Table 2 and label 9 is referred to in the comment.

Furthermore, 2D fingerprint plots were generated to quantify the intermolecular interaction in the crystal packing of complex 1 (Figure 8). It is evident that H···H contacts predominate, contributing 32.4% of total Hirshfeld surface area of the molecules. The second most significant interaction is Cl···H/H···Cl contributing 25.9%, which attributed to O–H···Cl and C–H···Cl H-bonding interactions, indicating two sharp symmetrical spikes in the 2D fingerprint plot. After that O···H/H···O interactions contributed 16.2%, which corresponds to the O–H···O H-bonding with symmetrical long sharp spikes in the 2D fingerprint plot. The presence of sharp symmetrical spikes shows the strong hydrogen bonding. Apart from the above, C···H/H···C (12%), C···C (6.6%), O···C/C···O (3.8%), C···N/N···C (1.5%) and N···H/H···N (0.4%) interactions were also evident.

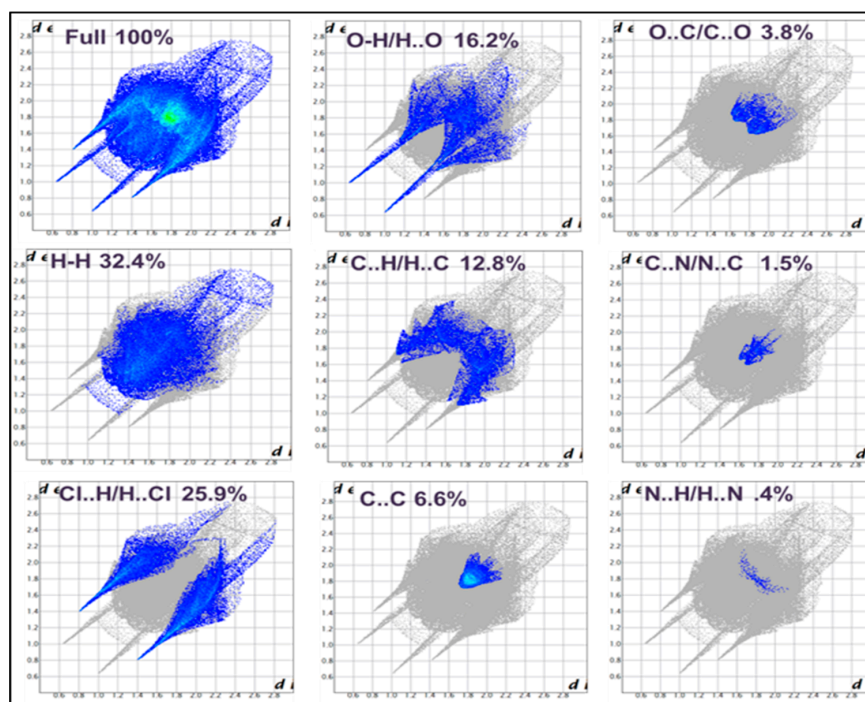


Figure 8. 2D fingerprint plots of complex 1.

3.6. Third-Order NLO and Optical Limiting Behavior

The third-order nonlinear optical behavior of complex 1 dissolved in ethanol has been explored using close and open aperture Z-scan methods at a solution concentration of 5.0 mM and input laser power of 100 mW. The recorded normalized transmittance corresponding sample position (Z) for closed aperture (CA) and open aperture (OA) have been depicted in Figure 9a,b respectively. Figure 9a, revealing the pre-focal peak and post-focal valley transmittance, demonstrates the self-defocusing nature of the sample. This peak-valley configuration is a clear indication of negative nonlinear refraction, ($n_2 < 0$), and it is attributed to thermal nonlinearity in the sample produced due to laser interaction [30]. The negative nonlinear refraction is payable to density changes of the medium, which overcome the positive sign of the transient orientational nonlinearity. In this situation, the measured transmittance remains constant as the sample approaches the beam focus and irradiance increases, leading to self-lensing in the sample [34]. Figure 9b reveals the minimum (valley) transmittance at focus, which suggests the reverse saturable absorption (RSA) nature of the sample. This reverse saturable absorption nature provides information about the positive nonlinear absorption in material, ($\beta > 0$).

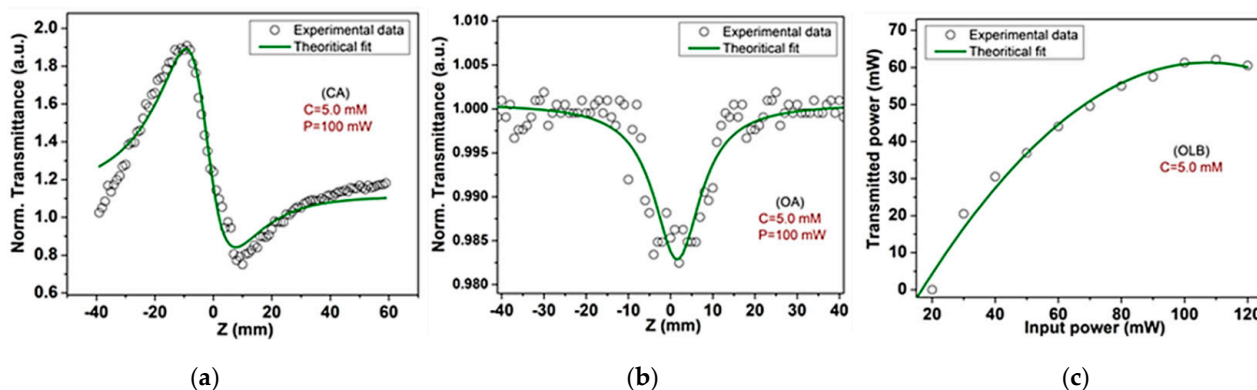


Figure 9. Normalized transmittance traces for (a) close aperture (CA) and (b) open aperture (OA), (c) optical limiting behavior (OLB).

The difference in normalized transmittance (ΔT_{P-V}) between peak and valley relates to the on-axis phase shift ($\Delta\Phi_0$) at the focus as

$$\Delta T_{P-V} = 0.406(1 - S)^{0.25} |\Delta\Phi_0|$$

The phase shift provides the nonlinear refractive index (n_2), and they are related as $|\Delta\Phi_0| = kn_2L_{\text{eff}}I_0$, where S represents the linear transmittance and is defined as $S = 1 - \exp(-2r_0^2/w_0^2)$, and r_0 , w_0 denote the radius of aperture and size of the laser beam at aperture entrance, respectively, and $k = \frac{2\pi}{\lambda}$ is the wavenumber corresponding to laser wavelength (λ). Further, the effective thickness (L_{eff}) for bulk of the materials with the optical path length, which is actual thickness (L_a) for thin films of the sample are related as $[1 - \exp(-\alpha_0L)]/\alpha_0$, where α_0 and I_0 are the linear absorption coefficient and peak intensity of laser beam, respectively. The on-axis intensity of the laser beam at the focus is defined as $I_0 = 2P/\pi\omega_0^2$, where P and ω_0 are the actual laser power and beam waist radius. The magnitude of n_2 is calculated doing theoretical fitting to the experimental CA normalized transmittance (T) using the following relations [35]

$$T(\text{close}) = 1 + \frac{2(-\rho x^2 + 2x - 3\rho)}{(x^2 + 9)(x^2 + 1)} \Delta\Phi_0$$

where ρ and x are the dimensionless parameters, defined as $\rho = \Delta\psi/\Delta\Phi_0$ and $x = Z/Z_R$, respectively, and $\Delta\psi$ is the phase shift at the focus due to nonlinear absorption and defined as ($\Delta\psi = \beta L_{\text{eff}}I_0/2$). The distances Z and Z_R are the sample positions along the laser beam axis and the Rayleigh diffraction length of the laser beam, respectively. The Rayleigh diffraction length is denoted as $Z_R = k\omega_0^2/2$.

To find out the nonlinear absorption coefficient (β), the theoretical fitting is performed on experimental OA normalized transmittance (T) using the following relations [30]

$$T(z, S = 1) = \sum_{m=0}^{\infty} \frac{[-q_0(z)]^m}{(m+1)^{3/2}}$$

This relation is valid for $q_0(0) < 1$, with $q_0(z) = \beta L_{\text{eff}}I_0 / (1 + z^2/Z_R^2)$.

The third-order nonlinear optical susceptibility, $\chi^{(3)}$, of material is calculated using the coefficients of nonlinear refraction (n_2) and nonlinear absorption (β). The nonlinear susceptibility is the combination of real and imaginary parts and it is defined as $\chi^{(3)} = \chi_R^{(3)} + i\chi_I^{(3)}$. The real, $\chi_R^{(3)}$ and imaginary, $\chi_I^{(3)}$ parts of $\chi^{(3)}$ are defined as

$$\begin{aligned} \chi_R^{(3)} &= 10^{-4} \frac{\epsilon_0 c^2 n_0^2}{\pi} n_2 (\text{cm}^2/\text{W}) \\ \chi_I^{(3)} &= 10^{-2} \frac{\epsilon_0 c^2 n_0^2 \lambda}{4\pi^2} \beta (\text{cm}/\text{W}) \end{aligned} \quad (1)$$

where, ϵ_0 , c and n_0 denote the permittivity of free space, speed of light in vacuum, and the coefficient of linear refraction of the material, respectively. The absolute value of nonlinear susceptibility is calculated as: $|\chi^{(3)}| = \sqrt{(\chi_R^{(3)})^2 + (\chi_I^{(3)})^2}$.

The enumerated third-order NLO characteristics of complex **1** are given in Table 3. The absolute values of third-order nonlinear optical characteristics of complex **1** are found to be comparable to those of reported Schiff base compounds measured in the CW regime as shown in Table 3. These outcomes of the NLO study for complex **1** reflect its potential applications for photonic and optoelectronic devices.

The optical limiting behavior (OLB) of complex **1** is represented in Figure 9c, where the transmitted power is measured corresponding to the laser input power at a solution concentration of 5.0 mM. The optical limiting character of complex **1** demonstrates that for lower input power the material shows full transparency, but it becomes opaque for higher

input power. The threshold limit and saturating limit of complex **1** are found to be 26 mW and 110 mW, respectively. This limiting behavior of complex **1** suggests its potential for instrumental protective devices against high laser illuminations.

Table 3. Third-order NLO characteristics of complex **1** and its ligand (H₂L) and comparison with other reported materials.

Materials	n_2 [cm ² /W]	$\chi_R^{(3)}$ [esu]	B [cm/W]	$\chi_I^{(3)}$ [esu]	$ \chi^{(3)} $ [esu]	References
Complex 1	-1.35×10^{-7}	-6.34×10^{-6}	2.63×10^{-4}	0.512×10^{-7}	6.36×10^{-6}	This work
H ₂ L	-1.89×10^{-7}	-9.59×10^{-4}	8.85×10^{-6}	[27]
BDMHC	1.00×10^{-9}	3.84×10^{-5}	1.24×10^{-7}	[16]

4. Conclusions

In this work, Zn(II) complex synthesized by using zwitterionic Schiff base ligand under reflux condition has been studied. Structural characterization revealed the Zn(II) complex occupied distorted trigonal bipyramidal geometry with Addison parameter $\tau = 0.68$. Moreover, Hirshfeld surface analysis showed that the most prominent interaction in the crystal packing is O–H...Cl, C–H...Cl and C–H... π interaction. PXRD data provides the bulk phase purity of complex **1** and thermal stability of the compound is reflected by its TGA analysis. The topological analysis of complex **1** was also performed in order to give deep insight into the role of H-bonding and other weak interactions involved in the supramolecular architecture of the Lewis acidic, zwitterionic Schiff base Zn(II) complex. The third-order non-linear properties of complex **1** were measured by Z-scan technique and it was found that the optical limiting character of complex **1** may provide its potential applications for instrumental protective devices against high laser illuminations.

Supplementary Materials: The following are available online at <https://www.mdpi.com/article/10.3390/cryst11050508/s1>. The details of X-ray crystal refinement, protocols related to topological and Hirshfeld surface analysis; Tables S1–S6; Selected bond lengths [Å], bond angles [°], Hydrogen atom coordinates, fractional atomic coordinates, anisotropic displacement parameters, multilevel analysis of molecular complex packing as monomer and dimer of complex **1**. Figure S1. IR spectrum of complex **1**; Figure S2. UV-Vis spectrum of complex **1**.

Author Contributions: All authors confirm that they have contributed reasonably, and take full accountability for the work, covering each part of the manuscript. All authors approve the corresponding authors (M.A. (Musheer Ahmad) & M.M. (Mohd. Muddassir)) as the representative person for the manuscript treatment. Validation, Preparation, creation and/or presentation of the published work, specifically writing the initial draft, S.K.; Validation, Formal analysis, M.M. (Mohd Mehkoom), and S.M.A.; Data curation, M.M. (Mohd Muslim); Methodology, Formal analysis, S.M.A.; Resources, S.M.A. and A.A. (Abdullah Alarifi); Writing—review & editing, M.A. (Mohd Afzal), Funding acquisition, M.M. (Mohd Muddassir); Project administration, M.M. (Mohd. Muddassir) and M.A. (Musheer Ahmad); Visualization, A.A. (Ahmad Alowais) and A.N.A. All authors have read and agreed to the published version of the manuscript.

Funding: The Department of Applied Chemistry, ZHCET, Faculty of Engineering and Technology, Aligarh Muslim University, UP, India (UGC Start-up grant). The authors are grateful to the Deanship of Scientific Research, King Saud University, for funding this work through group project number RG-1440-076. The author Saima Kamaal also grateful to UGC, India for providing Non-Net fellowship.

Data Availability Statement: Data is contained within the article or supplementary materials.

Conflicts of Interest: There are no conflict to declare.

References

- Castet, F.; Rodriguez, V.; Pozzo, J.-L.; Ducasse, L.; Plaquet, A.; Champagne, B. Design and Characterization of Molecular Nonlinear Optical Switches. *Acc. Chem. Res.* **2013**, *46*, 2656–2665. [[CrossRef](#)] [[PubMed](#)]
- Green, K.A.; Cifuentes, M.P.; Samoc, M.; Humphrey, M.G. Metal alkynyl complexes as switchable NLO systems. *Coord. Chem. Rev.* **2011**, *255*, 2530–2541. [[CrossRef](#)]

3. Sampath Kumar, H.C.; Ramachandra Bhat, B.; Rudresha, B.J.; Ravindra, R.; Philip, R. Synthesis, characterization of N,N'-bis(2-hydroxynaphthalidene)phenylene-1,2-diamine with M(II)(M=Ni, Zn and Fe) Schiff-base complexes and their non-linear optical studies by z-scan technique. *Chem. Phys. Lett.* **2010**, *494*, 95–99. [[CrossRef](#)]
4. Rottwitt, K.; Tidemand-Lichtenberg, P. *Nonlinear Optics: Principles and Applications*; CRC Press: Boca Raton, FL, USA, 2014.
5. Lolage, S.R.; Pawal, S.B.; Chavan, S.S. Azobenzene based Zn(II)/Ru(II) coordination-organometallic hybrid complexes: Influence of π -conjugation, donor/acceptor substituent's and coligands on electrochemical, luminescence and NLO properties. *Opt. Mater.* **2017**, *67*, 162–171. [[CrossRef](#)]
6. Chavan, S.S.; Bharate, B.G. Heterobimetallic M(II)/Ru(II) (M=Ni, Zn) complexes containing coordination and organometallic sites: Synthesis, characterization, luminescence and NLO properties. *Inorganica Chim. Acta* **2013**, *394*, 598–604. [[CrossRef](#)]
7. Lacroix, P.G.; Di Bella, S.; Ledoux, I. Synthesis and Second-Order Nonlinear Optical Properties of New Copper(II), Nickel(II), and Zinc(II) Schiff-Base Complexes. Toward a Role of Inorganic Chromophores for Second Harmonic Generation. *Chem. Mater.* **1996**, *8*, 541–545. [[CrossRef](#)]
8. Abdel Aziz, A.A.; Elantabli, F.M.; Moustafa, H.; El-Medani, S.M. Spectroscopic, DNA binding ability, biological activity, DFT calculations and non linear optical properties (NLO) of novel Co(II), Cu(II), Zn(II), Cd(II) and Hg(II) complexes with ONS Schiff base. *J. Mol. Struct.* **2017**, *1141*, 563–576. [[CrossRef](#)]
9. Sayin, K.; Karakaş, D.; Karakaş, N.; Sayin, T.A.; Zaim, Z.; Kariper, S.E. Spectroscopic investigation, FMOs and NLO analyses of Zn(II) and Ni(II) phenanthroline complexes: A DFT approach. *Polyhedron* **2015**, *90*, 139–146. [[CrossRef](#)]
10. Li, N.; Lu, J.; Li, H.; Kang, E.-T. Nonlinear optical properties and memory effects of the azo polymers carrying different substituents. *Dye. Pigment.* **2011**, *88*, 18–24. [[CrossRef](#)]
11. Xu, W.; Wang, W.; Li, J.; Wu, Q.; Zhao, Y.; Hou, H.; Song, Y. Two-photon absorption property and excellent optical limiting response of three Schiff base derivatives with large conjugated system. *Dye. Pigment.* **2019**, *160*, 1–8. [[CrossRef](#)]
12. Garnovskii, A.D.; Kharisov, B.I.; Blanco, L.M.; Sadimenko, A.P.; Uraev, A.I.; Vasilchenko, I.S.; Garnovskii, D.A. Review: Metal Complexes as Ligands. *J. Coord. Chem.* **2002**, *55*, 1119–1134. [[CrossRef](#)]
13. Chu, C.-C.; Chang, Y.-C.; Tsai, B.-K.; Lin, T.-C.; Lin, J.-H.; Hsiao, V.K.S. trans/cis-Isomerization of Fluorene-Bridged Azo Chromophore with Significant Two-Photon Absorbability at Near-Infrared Wavelength. *Chem. Asian J.* **2014**, *9*, 3390–3396. [[CrossRef](#)]
14. He, G.S.; Tan, L.-S.; Zheng, Q.; Prasad, P.N. Multiphoton Absorbing Materials: Molecular Designs, Characterizations, and Applications. *Chem. Rev.* **2008**, *108*, 1245–1330. [[CrossRef](#)] [[PubMed](#)]
15. Senge, M.O.; Fazekas, M.; Notaras, E.G.A.; Blau, W.J.; Zawadzka, M.; Locos, O.B.; Ni Mhuircheartaigh, E.M. Nonlinear Optical Properties of Porphyrins. *Adv. Mater.* **2007**, *19*, 2737–2774. [[CrossRef](#)]
16. Uthaya Kumar, M.; Pricilla Jeyakumari, A.; Anbalagan, G.; Shinde, V.; Sriram, S. Quantum chemical studies on synthesis, characterization and third order nonlinear optical properties of (E)-2-(benzo [d][1,3] dioxol-5-ylmethylene)hydrazinecarboxamide single crystal. *J. Mater. Sci. Mater. Electron.* **2019**, *30*, 11931–11944. [[CrossRef](#)]
17. Jia, J.-H.; Tao, X.-M.; Li, Y.-J.; Sheng, W.-J.; Han, L.; Gao, J.-R.; Zheng, Y.-F. Synthesis and third-order optical nonlinearities of ferrocenyl Schiff base. *Chem. Phys. Lett.* **2011**, *514*, 114–118. [[CrossRef](#)]
18. Bredas, J.L.; Adant, C.; Tackx, P.; Persoons, A.; Pierce, B.M. Third-Order Nonlinear Optical Response in Organic Materials: Theoretical and Experimental Aspects. *Chem. Rev.* **1994**, *94*, 243–278. [[CrossRef](#)]
19. Liaros, N.; Iliopoulos, K.; Stylianakis, M.M.; Koudoumas, E.; Couris, S. Optical limiting action of few layered graphene oxide dispersed in different solvents. *Opt. Mater.* **2013**, *36*, 112–117. [[CrossRef](#)]
20. Alizadeh, S.; Kösoğlu, G.; Erdem, M.; Açar-Selçüki, N.; Özer, M.; Salih, B.; Bekaroğlu, Ö. Synthesis, characterization, third-order non-linear optical properties and DFT studies of novel SUBO bridged ball-type metallophthalocyanines. *Dalt. Trans.* **2020**, *49*, 17263–17273. [[CrossRef](#)]
21. Maya, E.M.; García, C.; García-Frutos, E.M.; Vázquez, P.; Torres, T. Synthesis of Novel Push–Pull Unsymmetrically Substituted Alkynyl Phthalocyanines. *J. Org. Chem.* **2000**, *65*, 2733–2739. [[CrossRef](#)]
22. de la Torre, G.; Vázquez, P.; Agulló-López, F.; Torres, T. Role of Structural Factors in the Nonlinear Optical Properties of Phthalocyanines and Related Compounds. *Chem. Rev.* **2004**, *104*, 3723–3750. [[CrossRef](#)]
23. Das, S.; Nag, A.; Goswami, D.; Bharadwaj, P.K. Zinc(II)- and Copper(I)-Mediated Large Two-Photon Absorption Cross Sections in a Bis-cinnamaldiminato Schiff Base. *J. Am. Chem. Soc.* **2006**, *128*, 402–403. [[CrossRef](#)]
24. Ananthi, N.; Balakrishnan, U.; Velmathi, S.; Manjunath, K.B.; Umesh, G. Synthesis, Characterization and Third Order Non Linear Optical Properties of Metallo Organic Chromophores. *Opt. Photonics J.* **2012**, *02*, 40–45. [[CrossRef](#)]
25. Evans, C.; Luneau, D. New Schiff base zinc(II) complexes exhibiting second harmonic generation. *J. Chem. Soc. Dalt. Trans.* **2002**, 83–86. [[CrossRef](#)]
26. Kluska, K.; Adamczyk, J.; Krężel, A. Metal binding properties, stability and reactivity of zinc fingers. *Coord. Chem. Rev.* **2018**, *367*, 18–64. [[CrossRef](#)]
27. Kamaal, S.; Mehkoom, M.; Ali, A.; Afzal, S.M.; Alam, M.J.; Ahmad, S.; Ahmad, M. Potential Third-Order Nonlinear Optical Response Facilitated by Intramolecular Charge Transfer in a Simple Schiff Base Molecule: Experimental and Theoretical Exploration. *ACS Omega* **2021**. [[CrossRef](#)]
28. Kamaal, S.; Faizi, M.S.H.; Ali, A.; Ahmad, M.; Iskenderov, T. Crystal structure of 4-[(3-methoxy-2-oxidobenzylidene)azaniumyl] benzoic acid methanol monosolvate. *Acta Crystallogr. Sect. E Crystallogr. Commun.* **2018**, *74*, 1847–1850. [[CrossRef](#)]

29. Sheik-bahae, M.; Said, A.A.; Van Stryland, E.W. High-sensitivity, single-beam n_2 measurements. *Opt. Lett.* **1989**, *14*, 955. [[CrossRef](#)]
30. Sheik-Bahae, M.; Said, A.A.; Wei, T.-H.; Hagan, D.J.; Van Stryland, E.W. Sensitive measurement of optical nonlinearities using a single beam. *IEEE J. Quantum Electron.* **1990**, *26*, 760–769. [[CrossRef](#)]
31. El-Shishtawy, R.M.; Al-Zahrani, F.A.M.; Afzal, S.M.; Razvi, M.A.N.; Al-amshany, Z.M.; Bakry, A.H.; Asiri, A.M. Synthesis, linear and nonlinear optical properties of a new dimethine cyanine dye derived from phenothiazine. *RSC Adv.* **2016**, *6*, 91546–91556. [[CrossRef](#)]
32. Addison, A.W.; Rao, T.N.; Reedijk, J.; van Rijn, J.; Verschoor, G.C. Synthesis, structure, and spectroscopic properties of copper(II) compounds containing nitrogen–sulphur donor ligands; the crystal and molecular structure of aqua [1,7-bis(N-methylbenzimidazol-2'-yl)-2,6-dithiaheptane] copper(II) pe. *J. Chem. Soc. Dalt. Trans.* **1984**, 1349–1356. [[CrossRef](#)]
33. Maiti, M.; Sadhukhan, D.; Thakurta, S.; Roy, S.; Pilet, G.; Butcher, R.J.; Nonat, A.; Charbonnière, L.J.; Mitra, S. Series of Dicyanamide-Interlaced Assembly of Zinc-Schiff-Base Complexes: Crystal Structure and Photophysical and Thermal Studies. *Inorg. Chem.* **2012**, *51*, 12176–12187. [[CrossRef](#)] [[PubMed](#)]
34. Gómez, S.L.; Cuppo, F.L.S.; Figueiredo Neto, A.M. Nonlinear optical properties of liquid crystals probed by Z-scan technique. *Braz. J. Phys.* **2003**, *33*, 813–820. [[CrossRef](#)]
35. Liu, X.; Guo, S.; Wang, H.; Hou, L. Theoretical study on the closed-aperture Z-scan curves in the materials with nonlinear refraction and strong nonlinear absorption. *Opt. Commun.* **2001**, *197*, 431–437. [[CrossRef](#)]